Effective hydraulic properties of 3D virtual stony soils identified by inverse modeling

Mahyar Naseri[*], Sascha C. Iden, and Wolfgang Durner

Division of Soil Science and Soil Physics, Institute of Geoecology, Technische Universität Braunschweig, Germany

Corresponding author: m.naseri@tu-bs.de, Langer Kamp 19c, 38106 Braunschweig, Germany

s.iden@tu-bs.de, Langer Kamp 19c, 38106 Braunschweig, Germany

w.durner@tu-bs.de, Langer Kamp 19c, 38106 Braunschweig, Germany

Core Ideas

- Virtual stony soils with different rock fragment contents were generated in 3D using the Hydrus 2D/3D software.
- Evaporation experiments and unit-gradient experiments were numerically simulated.
- We used inverse modelling with the Richards equation to identify effective hydraulic properties of virtual stony soils.
- The identified hydraulic properties were used to evaluate the scaling models of calculating hydraulic properties of stony soils.

Abstract
Stony soils that have a considerable amount of rock fragments (RF) are widespread around the world. However, experiments to determine effective hydraulic properties of stony soils (SHP), i.e. the water retention curve (WRC) and hydraulic conductivity curve (HCC), are challenging. Installation of measurement devices and sensors in these soils is difficult and the data are less reliable because of their high local heterogeneity. Therefore, effective properties of stony soils especially in unsaturated hydraulic conditions are still not well understood. An alternative approach to

27 evaluate the SHP of these systems with internal structural heterogeneity is numerical simulation. We used the Hydrus

28 2D/3D software to create virtual stony soils in 3D and simulate water flow for different volumetric fractions of RF, f.

29 Stony soils with different values of f from 11 to 37 % were created by placing impermeable spheres as RF in a sandy

30 loam soil. Time series of local pressure heads in various depths, mean water contents, and fluxes across the upper

31 boundary were generated in a virtual evaporation experiment. Additionally, a multi-step unit gradient simulation was

32 applied to determine effective values of hydraulic conductivity near saturation up to $pF = 2$. The generated data were

33 evaluated by inverse modeling, assuming a homogeneous system, and the effective hydraulic properties were

34 identified. The effective properties were compared with predictions from available scaling models of SHP for different

35 values of f. Our results showed that scaling the WRC of the background soil based on only the value of f gives

36 acceptable results in the case of impermeable RF. However, the reduction of conductivity could not be simply scaled

37 by the value of f. Predictions were highly improved by applying the Novák, Maxwell, and GEM models to scale the

38 HCC. The Maxwell model matched the numerically identified HCC best.

39 **1. Introduction**

40 Stony soils are soils with a considerable amount of rock fragments (RF) and are widespread in mountainous and

41 forested watersheds around the world (Ballabio et al., 2016; Novák and Hlaváčiková, 2019). RF in soil are particles

42 with an effective diameter of larger than 2 mm (Tetegan et al., 2015; Zhang et. al., 2016). Their existence in soil

43 influences the two constitutive soil water relationships known as soil hydraulic properties (SHP) i.e. water retention

44 curve (WRC), and hydraulic conductivity curve (HCC) (Russo, 1988; Durner and Flühler, 2006). The accurate

45 identification of SHP is a prerequisite for adequate prediction of water flow in soil with the Richards equation

46 (Farthing and Ogden, 2017; Haghverdi et al., 2018). The SHP depend on soil texture and structure (Kutilek, 2004;

47 Lehmann et al., 2020), and are influenced by the presence of RF in soil. It is generally accepted that RF decrease the

48 water storage capacity of soils and its effective unsaturated hydraulic conductivity. In contrast, the formation of

49 macropores in the vicinity of embedded RF may lead to an increase in saturated hydraulic conductivity. While

50 experimental evidence and theoretical analyses show that the volumetric fraction of RF, f (v/v), has the highest

51 influence on effective SHP of stony soil, the effect of other characteristics of RF such as their porosity, shape, size,

52 arrangement, and orientation towards flow is less clear (Hlaváčiková and Novák, 2014; Hlaváčiková et al., 2016;

53 Naseri et al., 2020). Up to the present, two approaches have been dominant in identifying the hydraulic behavior of

54 stony soils: I) Experimental setups with the aim of measuring SHP of stony soils in the field or in controlled systems

55   in the laboratory (Cousin et al., 2003; Dann et al., 2009; Grath et al., 2015; Beckers et al., 2016, Naseri et al., 2019),

56   and II) Development of empirical, physical or physico-empirical approaches to scale hydraulic properties of

57   background soil based on the value of f and characteristics of RF (Novák et al., 2011; Naseri et al., 2020). These two

58   approaches have some systematic limitations that restrict their applications in investigating the hydraulic behavior of

59   stony soils. Installation of sensors and measurement instruments in the stony soils are technically demanding (Cousin

60   et al., 2003; Verbist et al., 2013, Coppola et al., 2013; Stevenson et al., 2021), undisturbed sampling is laborious

61   (Ponder and Alley, 1997), relatively larger samples are required (Germer and Braun, 2015), and the measured data

62   might be more inconsistent due to the higher local heterogeneity of such soils (Baetens et al., 2009; Corwin and Lesch,

63   2005). Furthermore, some of the available scaling models to obtain effective SHP are conceptually oversimplified and

64   they exclusively consider the value of f as the only input parameter (Bouwer and Rice, 1984; Ravina and Magier,

65   1984). Additionally, they assume impermeable RF and are proposed mainly for saturated flow conditions. These

66   scaling models need a systematic verification under variably-saturated conditions using experimental data or 3D

67   simulations. Some reviews of these models and their evaluation are available in the literature (Brakensiek et al., 1986;

68   Novák et al., 2011; Beckers et al., 2016; Naseri et al., 2019).

69   Hlaváčiková and Novák (2014) proposed a model to scale the HCC of the background soil, parametrized with the van

70   Genuchten–Mualem (van Genuchten, 1980) model, using the model of Bower and Rice (1984). Hlaváčiková et al.,

71   (2018) used the water content of RF as input parameter to scale the WRC of the background soil. Naseri et al. (2019)

72   used the simplified evaporation method (Peters et al., 2015) to determine experimentally the effective SHP of small

73   soil samples containing various amounts of RF. Their study criticizes the application of the scaling models developed

74   for saturated stony soils to unsaturated conditions and emphasizes the need to develop approaches that consider more

75   characteristics of the RF to calculate SHP of the stony soils.

76   Recent advancements in computational hydrology and computing power suggest the numerical simulation of soil

77   water dynamics as a promising alternative to the measurement of effective SHP of heterogeneous soils (Durner et al.,

78   2008; Lai and Ren, 2016; Radcliffe and Šimůnek, 2018). Numerical simulations have several advantages. They do not

79   demand strict experimental setups, are repeatable under a variety of initial and boundary conditions, and in contrast

80   to the laboratory experiments, space and time scales are not restrictive factors in the simulations. These assets have

81   made them a favorable tool in water and solute transport modeling in heterogeneous soils (Abbasi et al., 2003;

82   Šimůnek et al., 2016). However, with few exceptions, heterogeneous soils like stony soils have been simulated only

83   for simplified cases, i.e., either under fully saturated conditions or with reduced dimensionality, i.e., simulations of

84   stony soils in two spatial dimensions (2D). Novák et al. (2011) calculated effective saturated hydraulic conductivity

85   (K_s) of soils containing impermeable RF using steady-state simulations with the software Hydrus 2D which solves the

86   Richards equation in two spatial dimensions. They derived a linear relationship between K_s of stony soils and f.

87   Hlaváčiková et al. (2016) simulated different shapes and orientations of RF in Hydrus 2D to obtain the effective K_s of

88   the virtual stony soils. Beckers et al. (2016) used Hydrus 2D simulations to extend the investigations towards the

89   impact of f, shape, and size of RF on the HCC. They also identified effective SHP of a clay stony soil using laboratory

90   evaporation experiments for f values up to 20 % (v/v).

91   The inverse modeling approach has been applied to identify effective hydraulic properties of soils in laboratory

92   experiments (Ciollaro and Romano, 1995; Hopmans et al., 2002; Nasta et al., 2011), in lysimeters and field (Abbaspour

93   et al., 1999; Abbaspour et al., 2000), virtual lysimeters with internal textural heterogeneity (Durner et al., 2008; Schelle

94   et al., 2013), and WRC of stony soils through field infiltration experiments (Baetens et al., 2009). Although theoretical

95   studies and laboratory investigations on packed samples are insufficient to understand fully the hydraulic processes in

96   stony soils, they do lead the way to the improvement and validation of effective models and their application at the

97   field and even larger scales. Inverse modeling is arguably the best approach to achieve these aims because it allows to

98   validate effective models using process modeling. Our aim in this study was to investigate the application of inverse

99   modeling to identify the effective SHP of 3D virtual stony soils and to explore its applicability to these soil systems

100 as an example of internal structural heterogeneity. We were interested in answering the following questions:

101 i) Is it possible to describe the dynamics in the heterogeneous 3D system with the 1D Richards equation assuming a

102 homogeneous soil?

103 ii) If so, what are the effective SHP of stony soils and how do they relate to the SHP of the background soil?

104 To answer these questions we conducted forward simulations of water movement in 3D using the Richards equation

105 as variably-saturated flow model. We created stony soils by embedding voids representing impermeable spherical RF

106 as inclusions into a homogeneous background soil. Then we simulated transient evaporation experiments and stepwise

107 steady-state, unit-gradient infiltration experiments in 3D. The generated data were used as an input to a 1D inverse

108   model to obtain the effective SHP of stony soils, and these properties were used to evaluate and compare the available

109   scaling models of SHP for stony soils.

110   **2. Materials and methods**

111   **2.1. Simulation model**

112   The Hydrus 2D/3D software was used to generate virtual stony soils and simulate the water flow in the created three-

113   dimensional geometries. Water flow in Hydrus 2D/3D is modelled by the Richards equation (Šimůnek et al., 2006;

114   2008), which is the standard model for variably-saturated water flow in porous media. The Hydrus 2D/3D software

115   solves the mixed form of the Richards equation numerically using the finite-element method and an implicit scheme

116   in time (Celia et al., 1990; Šimůnek et al., 2008; 2016; Radcliffe and Šimůnek, 2018). The three-dimensional form of

117   the Richards equation under isothermal conditions, without sinks/sources, and assuming an isotropic hydraulic

118   conductivity is:

$$\frac{\partial \theta}{\partial t} = \frac{\partial}{\partial x}\left[K(h)\left(\frac{\partial h}{\partial x}\right)\right] + \frac{\partial}{\partial y}\left[K(h)\left(\frac{\partial h}{\partial y}\right)\right] + \frac{\partial}{\partial z}\left[K(h)\left(\frac{\partial h}{\partial z} + 1\right)\right] \tag{1}$$

119   where θ is the volumetric water content (cm^3 cm^{-3}), t is time (s), h is the pressure head (cm), and $K(h)$ is the hydraulic

120   conductivity function (cm d^{-1}). x, and y (cm) are the horizontal Cartesian coordinates, and z (cm) is the vertical

121   coordinate, positive upwards. We used the van Genuchten-Mualem model to parametrize the WRC and HCC (van

122   Genuchten, 1980):

$$S_e(h) = \frac{\theta(h) - \theta_r}{\theta_s - \theta_r} = [1 + (\alpha h)^n]^{-m} \tag{2}$$

123   and

$$K(h) = K_s S_e^\tau \left[1 - \left(1 - S_e^{\frac{1}{m}}\right)^m\right]^2 \tag{3}$$

124   where θ_s and θ_r are the saturated and residual water contents (cm^3 cm^{-3}), respectively, $S_e(h)$ is the effective saturation

125   (-), α (cm^{-1}) is a shape parameter, n is an empirical parameter related to the pore size distribution (-) and $m = 1 -$

126    $1/n$, K_s is the saturated hydraulic conductivity and τ is a tortuosity/connectivity parameter (-).

2.2. 3D geometries representing stony soils

The virtual stony soils in 3D were created by placing spherical inclusions in a background soil. In accordance with real laboratory experiments (not reported here), we generated virtual soil columns as cylinders with a diameter of 16 cm and a height of 10 cm and an total volume of ≈ 2011 cm^3. The inclusions were considered as voids representing impermeable RF embedded in the background soil. Configurations and characteristics of the created 3D geometries of stony soils are illustrated in Fig. 1. Each spherical inclusion had a diameter of 3.04 cm and a volume of ≈ 14.7 cm^3. Stony soils with different values of f were created by including different numbers of spherical inclusions in the soil column. A total number of 15, 27, 39, and 51 spherical inclusions in each column led to four volumetric RF contents of 11.0, 19.8, 28.5 and 37.3 % (v/v). Spheres were arranged in the column in three layers. The spheres' centers were in depths of 2.5, 5.0 and 7.5 in the column and each layer was packed with one-third of the total number of intended spheres. Furthermore, observation points at selected nodes of the numerical grid were inserted in each of the three depths of the column (i.e. 2.5, 5.0 and 7.5 cm) in the background soil and not in close vicinity of the inclusions to provide time series of soil water pressure head for the inverse simulations. For the background soil, a homogenous sandy loam soil was considered with the van Genuchten-Mualem model parameters $\theta_s = 0.410$ (cm^3 cm^{-3}), $\theta_r = 0.065$ (cm^3 cm^{-3}), $\alpha = 0.01$ (cm^{-1}), $n = 2.0$ (-), $\tau = 0.5$ (-), and $K_s = 100$ (cm d^{-1}). The targeted mesh size for the different simulations was set to 0.25 cm. The dependency of the numerical solution on the mesh size was tested with some refined meshes and negligible differences in the results were obtained for different mesh sizes.
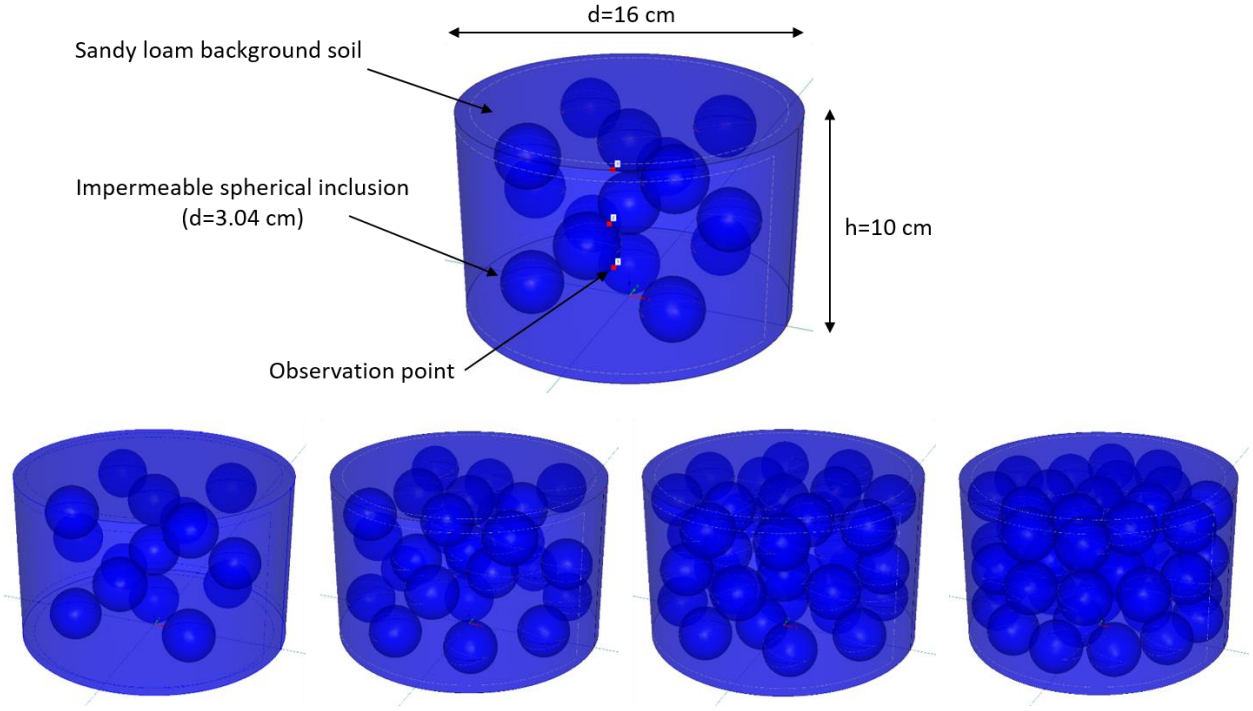
Figure 1: Visualization of the generated stony soils in 3D, including the dimension of RF and soil cylinder and location of the observation points (top). Bottom row shows the RF contents of 11.0, 19.8, 28.5 and 37.3 %, from left to right.

2.3. Forward simulations

We simulated evaporation (EVA) (Peters and Durner, 2008) and multistep unit gradient (MSUG) experiments (Sarkar et al., 2019). For EVA, a linear distribution of pressure head (-2.5 cm top, +7.5 cm bottom) was used as the initial condition. The boundary conditions were no-flux at the bottom and atmospheric with a constant potential evaporation rate of 0.6 (cm d^{-1}) and zero precipitation at the top. The EVA experiments were simulated for 10 days and the time series of pressure heads at each observation point, the initial volumetric water content and the cumulative evaporation and evaporation rate were collected for later use in the inverse simulations.

In the virtual MSUG experiment, the soil column was initially fully saturated with a constant pressure head of 0 cm. A sequence of step-wise decreasing constant pressure heads was assigned to the upper and lower boundaries of the column. The duration of the virtual MSUG experiment was 100 days and the pressure head in the upper and lower boundaries was simultaneously decreased stepwise to a pressure head of -100 cm. The applied pressure heads h_i were 0, -1, -3, -10, -20, -30, -60, and -100 cm, respectively. Time steps were chosen such that a steady-state flow condition was reached for each pressure step, indicated by identical water fluxes at the top (inflow) and bottom (outflow)

161   boundaries and constant pressure heads at the observation points. The hydraulic conductivities at the respective

162   pressure heads h_i data were calculated by dividing the steady-state water flux rates ($cm^3\ d^{-1}$) by the total surficial area

163   of the soil column ($\approx 202\ cm^2$).

164   The converging and diverging flow field around obstacles produces even under unit gradient conditions spatially

165   different pressure heads, and as opposed to saturated conditions, these different pressure heads are under unsaturated

166   conditions associated with different water saturations and different local hydraulic conductivities. We were interested

167   in whether and to what extent this could lead to nonlinear effects in the derivation of the effective hydraulic properties,

168   in particular the effective HCC. Furthermore, since the flow field for a given volume fraction of obstacles depends on

169   dimensionality, i.e., is different in a 2D simulation than in a 3D simulation, studying the effects in the unsaturated

170   region was one of the main motivations for performing this numerical analysis in 3D.

171 **2.4. Inverse modeling of evaporation in 1D**

172   A 10-day EVA experiment in 1D was simulated with the software package Hydrus-1D (Šimůnek et al., 2006; 2008)

173   to obtain the SHP parameters using inverse modeling. The generated data from the EVA and MSUG forward

174   simulations in 3D were used as input to the 1D inverse simulations. Time series of the pressure heads at three

175   observation depths, mean volumetric water contents in the column during the virtual EVA experiment, and the data

176   points of the effective HCC from the virtual MSUG experiment were used in the objective function. The time series

177   of the mean volumetric water content was calculated from the initial water content, cumulative evaporation and soil

178   volume. The measurement range for pressure heads used in the objective function was from saturation down to -2000

179   cm. This reflects a setup with laboratory tensiometers with boiling delay (Schindler et al., 2010). The time series of

180   the simulated evaporation rates from the 3D simulations were used as the time variable atmospheric boundary

181   condition for the 1D inverse simulations. The 1D soil profile was 10 cm long, and was discretized into 100 equally

182   sized finite elements. Similar to the 3D simulations, three observation points were defined in the depths of 2.5, 5.0

183   and 7.5 cm. A no-flux boundary condition was used at the bottom. The six parameters of the van Genuchten model

184   occurring in Eq. (2) and (3) were all simultaneously estimated by inverse modeling. The weighted-least-squares

185   objective function was minimized by the SCE-UA algorithm (Duan et al., 1992). The data obtained from the EVA

186   experiment allow to identify the WRC from saturation to the pressure where the tensiometers fail, and the HCC in the

187   mid to dry range of the SHP (roughly between -100 to -2000 cm pressure heads), while the MSUG provides a precise

188   determination of the HCC in the wet range (Sarkar et al., 2019; Durner and Iden, 2011). The EVA experiments do not

189   provide information on hydraulic conductivity near water-saturation (Peters et al., 2015). Therefore, we included the

190   obtained data from the virtual MSUG experiment in the object function for the inverse simulation of the virtual EVA

191   experiments, to improve the uniqueness of the inverse solution and the precision of the identified HCC near saturation

192   (see Schelle et al., 2010, for another example).

193   **2.5. Predicting SHP of virtual stony soils by scaling models**

194   The SHP of stony soils obtained by inverse modeling were compared to SHP that are predicted by available scaling

195   models and used for their evaluation. Considering that f has the dominant influence on the WRC of a stony soil, a

196   common approach is partitioning the WRC and HCC of stony soil based on the volume of each component in the soil-

197   rock mixture and calculating the effective SHP of stony soil using the volume averaging or the composite-porosity

198   model. The general form of the WRC model considers the moisture contents of the background soil θ_{soil} (h) (cm^3 cm$^-$

199   ^{3}) and embedded rock fragments θ_{rock} (h) (cm^3 cm^{-3}) to calculate the effective WRC of stony soils θ_m(h) (cm^3 cm^{-3})

200   (Flint and Childs, 1984; Peters and Klavetter, 1988) with the following form in the full moisture range (Naseri et al.,

201   2019):

$$\theta_m(h) = f\theta_{rock} + (1-f)\theta_{soil} \tag{4}$$

202   A typical assumption in stony soils hydrology is that the porosity of RF is negligible. In this case, Eq. (4) reduces to

203   (Bouwer and Rice, 1984):

$$\theta_m(h) = (1-f)\theta_{soil} \tag{5}$$

204   For the effective hydraulic conductivity of stony soils, some scaling models are developed for saturated conditions

205   that might apply to the hydraulic conductivity at any pressure heads. The simplest scaling model accounts only for the

206   reduction in the cross-sectional area available for flow of water. This leads to the equation (Ravina and Magier, 1984):

$$K_r = 1 - f \tag{6}$$

207   where K_r (-) is the relative hydraulic conductivity of stony soil, i.e., $K_r = K_m/K_{soil}$, where K_m is the effective hydraulic

208   conductivity of the stony soil (cm d^{-1}), and K_{soil} is the conductivity of the background soil (cm d^{-1}).

209 Ina more recent approach, Novák et al. (2011) developed a linear relationship based on the 2D numerical simulation

210 results as a first approximation to scale the saturated hydraulic conductivity of stony soils:

$$K_r = 1 - \alpha f \qquad (7)$$

211 The parameter α was reported to depend on the texture of the background soil, with a range between 1.1 for sandy

212 clay to 1.32 for clay. This model is easy to apply, but it requires the estimation of the parameter α to calculate K_r. For

213 our calculations, we assumed $\alpha = 1.2$ for the sandy loam background soil used in our study.

214 Another model that has been developed for mixtures with spherical inclusions is the Maxwell model (Maxwell, 1873;

215 Corring and Churchill, 1961; Peck and Watson, 1979; Zimmermann and Bodvarsson, 1995). It takes the value of f,

216 hydraulic conductivity of the background soil and hydraulic conductivity of inclusions into account to calculate the

217 hydraulic conductivity of the stony soil. In the special case of impermeable inclusions, Maxwell model reduces to:

$$K_r = \frac{2(1-f)}{2+f} \qquad (8)$$

218 A recently developed model by Naseri et al. (2020), which is based on the general effective medium theory (GEM),

219 allows considering effects of permeability, shape, and orientation of RF on the effective HCC. For impermeable RF,

220 the GEM model reduces to the following form:

$$K_r = \left(1 - \frac{f}{f_c}\right)^t \qquad (9)$$

221 where f_c is the critical f with values between 0.84 and nearly 1 and t is a shape parameter with values between 1.26

222 and nearly 1.5 for spherical RF. In this study, we set $f_c = 0.982$ (v/v) according to the size ratio of the RF to the

223 background soil, and $t = 1.473$ for spherical RF (for details, see appendix in Naseri et al., 2020).

224 It should be noted that all approaches apply at any pressure head h_i, i.e., the scaling that is originally developed for

225 saturated conditions with locally constant hydraulic conductivity in the background soil is equally applied to

226 unsaturated conditions.

3. Results and discussion

3.1. Flow field and variability of state variables in the virtual MSUG experiment

Figure 2 visualizes the pressure head (cm), water content (cm^3 cm^{-3}), and velocity (cm d^{-1}) in a 2D cross section in the center of the soil column through the forward simulation of the MSUG experiment. The profile is shown for the steady state flux situation with a pressure head of -100 cm and the stony soil with $f = 28.5$ %. The Figure shows a considerable change in the flow velocities, even at the upper boundary. Also, as Fig. 2 illustrates, the conditions above an obstacle might be slightly wetter than below an obstacle, but the variations in the pressure head and the water content fields is very small. We note that this general finding was equally applicable for all other pressure heads steps in the virtual MSUG experiment.
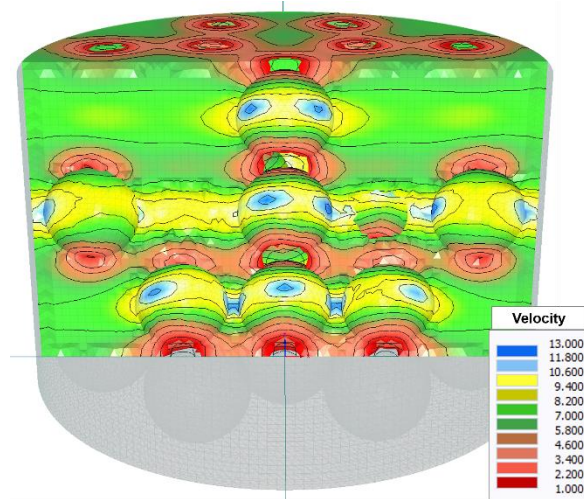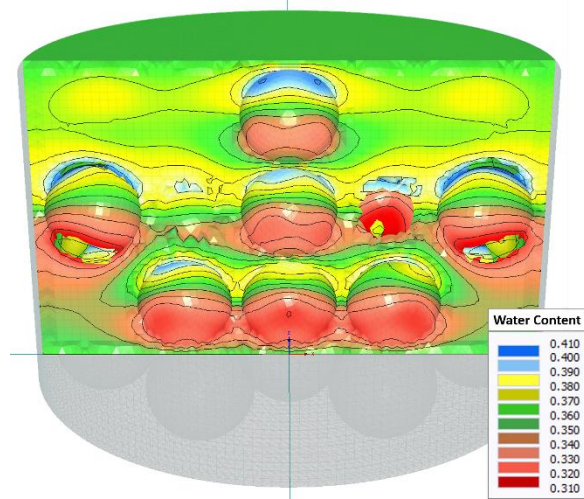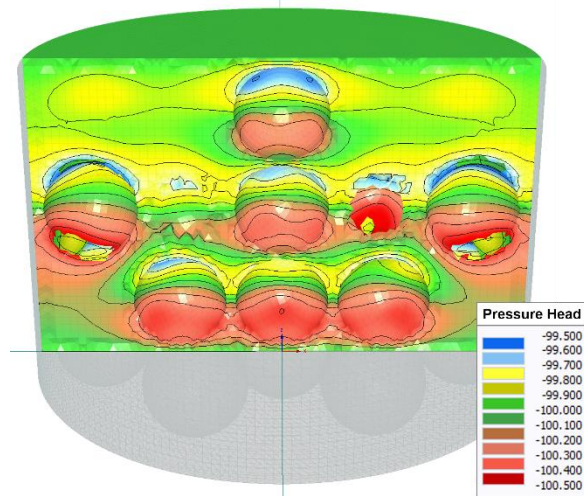
237

238

239

240 *Figure 2: Visualization of the pressure head (cm), water content ($cm^3\ cm^{-3}$), and velocity ($cm\ d^{-1}$) in a 2D profile in the center of*
241 *the soil column during the forward simulation of MSUG experiment.*

242   **3.2. Comparison of the relative K_s of the scaling models and the 3D simulations under saturated conditions**

243   The dependency of the relative saturated hydraulic conductivity (K_r) on the percentage of RF, calculated by different

244   scaling models and the obtained values from the first pressure in the virtual MSUG experiment is presented in Fig. 3.

245   The results of the models are shown up to the $f = 37.3$ %, which was the highest value of f simulated in 3D. However,

246   some of the evaluated models are theoretically valid for higher or lower values of f, e.g. 40 % for the Novák et al.

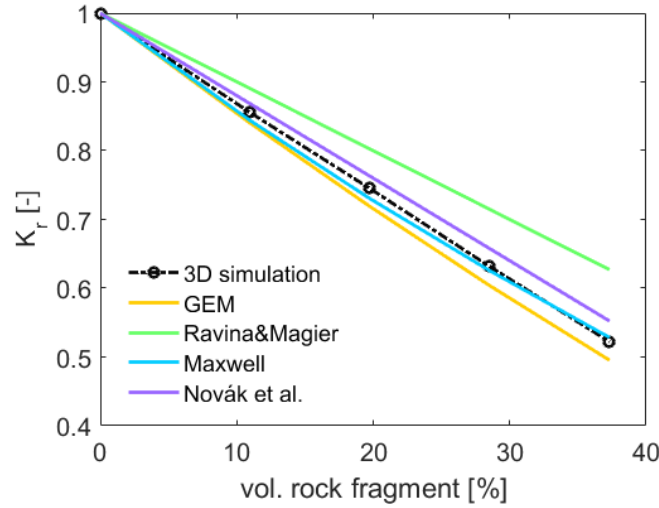247   (2011) model and higher values for the GEM model (Naseri et al., 2020).

248

249   *Figure 3: Comparison of the values of K_r (-) from the virtual MSUG experiment in 3D (circles), and calculated by different scaling*
250   *models (solid lines) for f values up to 37.3 %. The dashed line connects the simulated data points of K_r shown by circles.*

251   Obviously, the results of our simulations confirm a linear reduction of K_r with increasing the volume of RF up to $f =$

252   37.3 % (v/v) in the soil. The numerically obtained values of K_r are shown by circles and connected by the dashed line

253   in Fig. 3. The dashed line has a slope of -1.29 representing a higher reduction rate of K_r compared to the scaling of K_r

254   that would be proportional to f, expressed by Eq. (6) and predicted by the model of Ravina and Magier (1984) (solid

255   green line). This result supports the fact that even in a stony soil with spherical impermeable RF, the reduction in the

256   hydraulic conductivity is higher than the reduction of the average cross-sectional area (which is statistically equivalent

257   to the value of f). Hlaváčiková et al. (2016) found an even higher value of -1.45 for spherical RF with a diameter of

258   10 cm. The model of Novák et al. (2011) performs better but also leads to a slight under-prediction of the reduction

259   of the effective saturated conductivity. The performance of this model could be improved by adjusting the parameter α

260   to match data of the 3D simulation, but doing this would lead to an unfair comparison with the other models. The two

261 models predicting a nonlinear relationship between the K_r and f, GEM and Maxwell, show similar results at low

262 contents of RF up to 10 %, with minor differences in outputs of the models. Among all of the evaluated models of

263 scaling K_s, the Maxwell model yields the closest match to the numerically identified values of K_r.

264 We note that these results may differ in natural soils, where an increase of the saturated hydraulic conductivity might

265 be expected because of macropore flow in lacunar pores at the interface between background soil and RF (Beckers et

266 al., 2016; Hlaváčiková et al., 2019, Arias et al., 2019). We have not included such a process in our 3D simulations.

267 **3.3. Inverse modeling results for effective hydraulic properties**

268 The observed and fitted time series of the pressure heads at the three representative observation points is shown in

269 Fig. 4 for the simulated experiments of the four cases with different values of f. In each case, the fitted pressure heads

270 at the three depths of the column (2.5, 5.0 and 7.5 cm) match well with the time series of the corresponding data from

271 the 3D virtual experiments. Specifically, the match of the pressure heads at 7.5 and 5.0 cm is excellent, whereas there

272 are slight systematic deviations at the uppermost level at the later stage of the virtual EVA experiment.
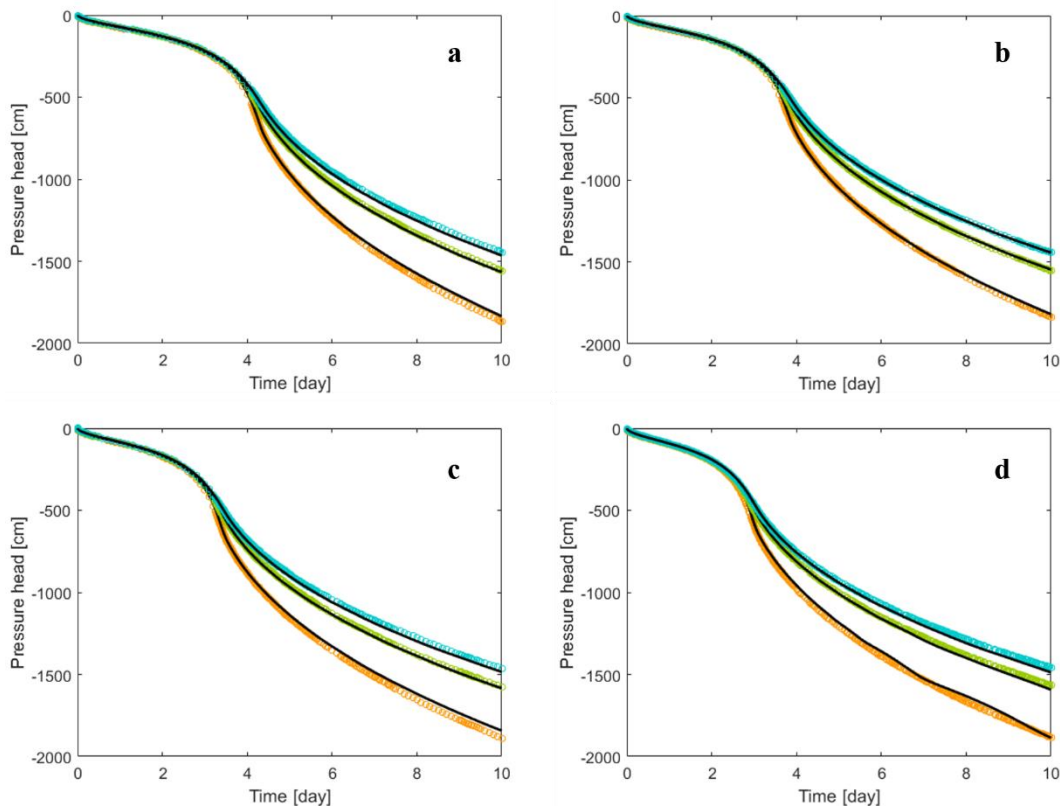
273

Figure 4: The time series of the 3D-simulated (circles) and 1D fitted (solid lines) pressure heads at the observation points in three
275 *depths of the stony soil columns with the f values a) 11.0 %, b) 19.8 %, c) 28.5 %, and d) 37.3 %. The observation depths are*
276 *indicated by different color codes of orange (upper, 2.5 cm), green (middle, 5.0 cm) and blue (lower, 7.5 cm from top).*

277

278   Table 1 shows the values of the root mean square error (RMSE) and mean absolute error (MAE) between the observed

279   and fitted time series of the pressure heads at three observations points for values of f. According to the Table 1, the

280   fit is best for the lower f and in the middle of the column. The highest deviations occur for the highest f but there is

281   no clear trend. Overall, the values of RMSE and MAE are in an acceptable range regarding the observed values of

282   pressure heads up to -2000 cm. This indicates that the time series of the pressure heads at multiple depths generated

283   by the 3D simulations of EVA experiments can be described successfully by the 1D Richards equation assuming a

284   homogenous system with effective SHP.

285

286   *Table 1: The values of RMSE and MAE between the observed and fitted pressure heads, in three observation points for different*
287   *values of f.*

Criteria	Observation point	Volumetric fraction of RF, f (%)			
		11.0	19.8	28.5	37.3
RMSE	upper	12.8	6.5	12.6	18.9
	middle	4.9	2.8	5.3	10.7
	lower	9.1	3.1	8.7	13.9
MAE	upper	10.0	4.9	9.4	14.5
	middle	4.0	2.1	4.5	8.5
	lower	7.0	2.6	6.8	11.0

288

289   The identified SHP are presented in Fig. 5. The solid lines in the Figure show the WRC and HCC of the virtual stony

290   soils obtained by inverse simulation (except the solid black lines, which are the WRC and HCC of the background

291   soil), the dashed lines represent the scaled WRC by Eq. (5) and HCC by Eq. (6), and the circles on the HCC plots

292   represent the discrete data points of hydraulic conductivity obtained by the virtual MSUG experiment. The WRC and

293   HCC are presented on a pF scale, which is defined as $pF = \log 10 (|h|)$, in which h is the pressure head in cm

294   (Schofield, 1935). The van-Genuchten model parameters of the background soil and stony soils are shown in Table 2.
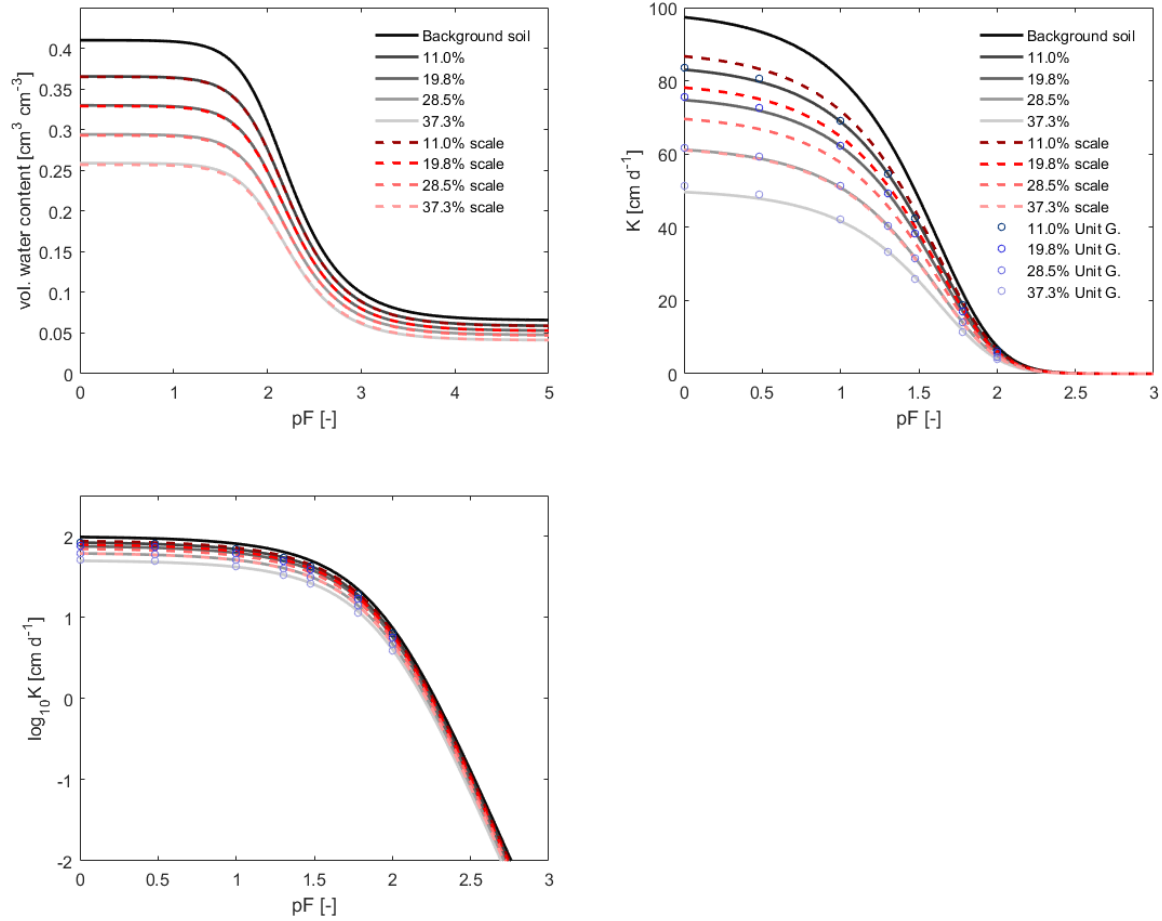
295

296

Figure 5: The WRC and HCC of the background soil (solid black line), and identified effective WRC (left) and HCC (right) of the
virtual stony soils (solid gray lines) with different values of f. The HCC are presented also in the logarithmic scale. The dashed
lines show the effective WRC and HCC calculated by the models of Bouwer and Rice (1984) and Ravina and Magier (1984). The
circles on the HCC present the data points of hydraulic conductivity obtained by the virtual MSUG experiment in near-saturated
conditions up to the $pF \approx 2$.

Table 2: The van-Genuchten model parameters of the SHP of the background soil and of the inversely determined effective SHP of
the virtual stony soils with different values of f.

Parameter	Unit	Volumetric fraction of RF, f (%)				
		Background soil	11.0	19.8	28.5	37.3
θ_s	(cm^3 cm^{-3})	0.410	0.365	0.330	0.294	0.259
θ_r	(cm^3 cm^{-3})	0.065	0.059	0.053	0.048	0.041
α	(cm^{-1})	0.010	0.010	0.010	0.010	0.010
n	(-)	2.000	2.007	2.011	2.014	2.037
K_s	(cm d^{-1})	100.0	84.7	76.2	62.3	50.4
τ	(-)	0.50	0.43	0.47	0.42	0.38

305

16

306   According to the Fig. 5 and Table 2 the value of the shape parameter α is independent of the value of f and the change

307   in the value of n is negligible (but might be systematic). The inversely identified WRC and the predictions from the

308   Bouwer and Rice (1984) scaling model match almost perfectly for all the RF contents. In agreement with this, there

309   is also an excellent agreement of the values of the saturated (θ_s) and residual water contents (θ_r) (cm^3 cm^{-3}) between

310   scaled and identified WRC. The values of θ_s and θ_r in the WRC are directly related to the values of f and the respective

311   values of the background soil and the WRC is scaled by this factor over the whole range of soil water pressure head.

312   Similar to the WRC, an increase of f reduces the hydraulic conductivity over the whole range of pressure head covered

313   by the virtual experiments. However, in contrast to the WRC, the simple scaling model based on Eq. (6) cannot

314   describe the reduction in HCC. Figure 5 shows that the model of Ravina and Magier (1984, dashed lines)

315   underestimates the reduction of the effective HCC for all RF contents. The reason might be related to the local

316   variations of the flow velocity in the soil column. It was shown in Fig. 2 that the variations in the water flow velocity

317   might be considerable. The nonlinearities in the flow field and changes in the local conductivities, together with an

318   increased average flow path length, force a stronger overall conductivity reduction. The arrangement of RF thus might

319   affect the reduction in hydraulic conductivities, leading to different conductivities at the same value of f (Naseri et

320   al., 2020). The degree depends on how the flow area is altered in the soil column due to the presence of RF (Fig. 1

321   and 2). This result is in agreement with Novák et al. (2011) who reported a higher reduction in conductivity compared

322   to a reduction that is proportional to the RF content. Furthermore, it may also differ alter depending on the

323   characteristics of RF such as their size, shape and orientation towards flow (Novák et al., 2011).

324   We had to include the data points of hydraulic conductivity from the virtual MSUG experiment in the inverse objective

325   function to get a precise identification of the HCC obtained by inverse modeling near saturation. The information

326   content from the virtual EVA experiment gives a unique identification only when the flux rate in the system reaches

327   the magnitude of the unsaturated hydraulic conductivity, which is for many soils around $pF = 1.5$ to $pF = 2$ (Peters

328   and Durner, 2008). Although there are some discrepancies visible near saturation for the case with a high value of f,

329   the resulting values of hydraulic conductivity from the virtual MSUG experiment and the inversely identified HCC

330   using the virtual EVA experiment join well around $pF = 2$ for all of the values of f. Therefore, the HCC could be

331   described successfully from the saturation up to $pF = 3$ using the inverse modeling of the virtual EVA experiment

332   with added K support points from the virtual MSUG experiment. The overall results suggest that the effective

333 hydraulic parameters of stony soils could be obtained by the corresponding real experiments and the result is robust

334 for both, WRC an HCC, even if the uncertainty in the identified HCC is higher than that of the WRC (Singh et al.,

335 2020; 2021).

336 **3.4. Evaluation of the Novák, Maxwell and GEM models using the identified HCC**

337 As stated above, the model of Ravina and Magier (1984) which is a linear scaling approach of the hydraulic

338 conductivity (Eq. 6) underestimates the reduction of conductivity in the stony soil. We used the identified HCC as a

339 benchmark to evaluate and compare more advanced models of scaling HCC, namely the Novák, Maxwell and GEM

340 models (Eq. 7, 8 and 9). Figure 6 illustrates the calculated HCC of stony soils with different values of f using these

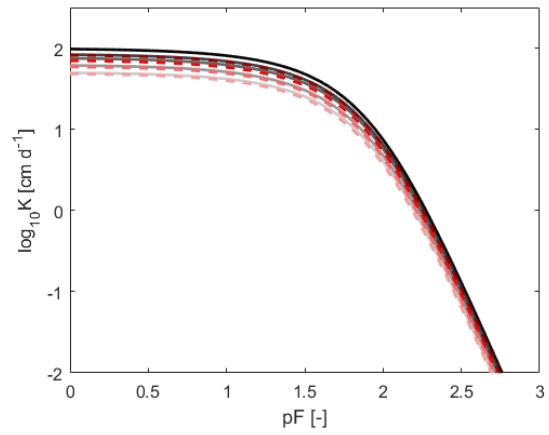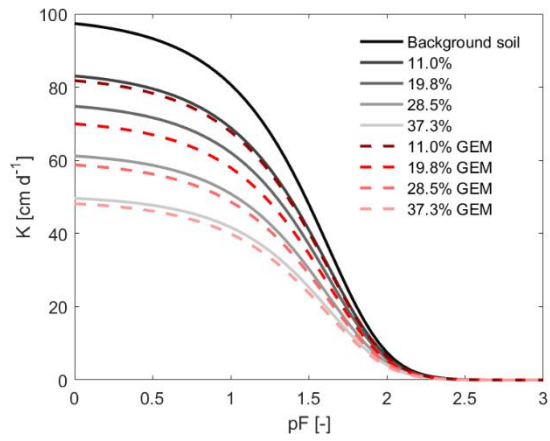341 models of scaling HCC and compares them to the identified HCC by the inverse modeling.
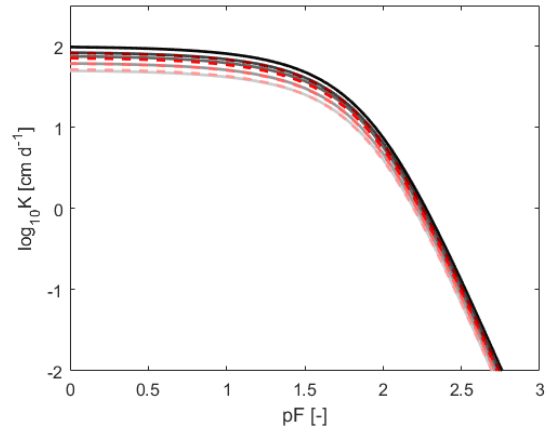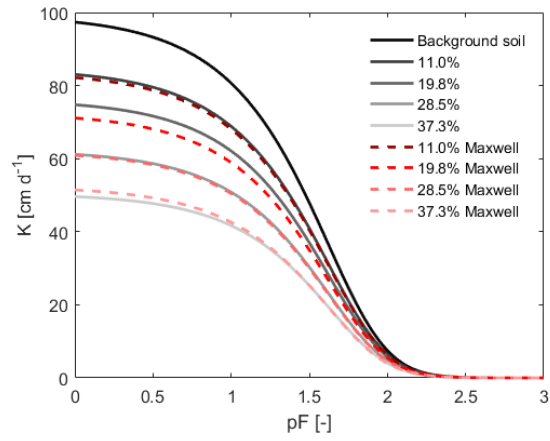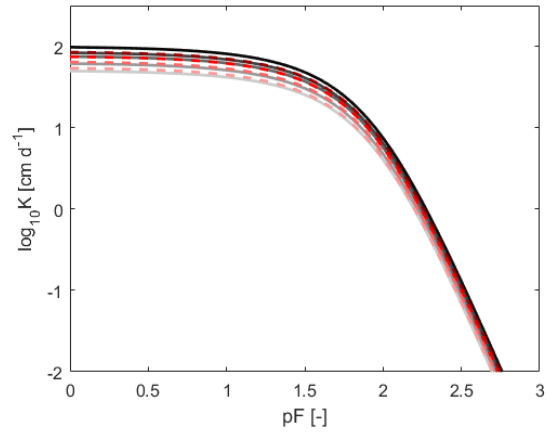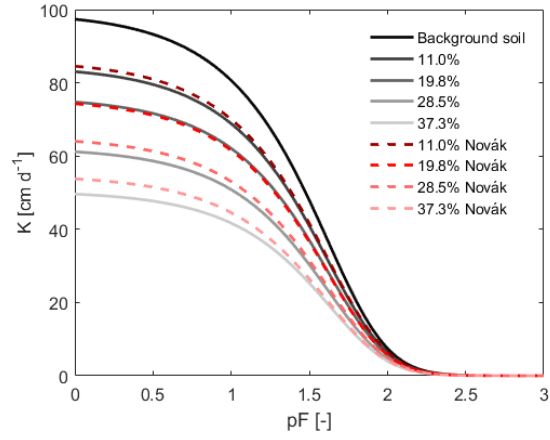
342

343

344

Figure 6: Evaluation of the Novák, Maxwell and GEM models of scaling HCC of stony soils using the identified HCC as a benchmark. The HCC in each case were obtained for f=11.0, 19.8, 28.5 and 37.3 % (v/v). The inverse identified curves are shown in solid lines and the model results in dashed lines. The value of f_c in the GEM model was set as 0.982 with the corresponding shape parameter t=1.473 and the parameter $\alpha = 1.2$ was selected for the Novák model.

349

350   The calculated HCC by the three models are in general in good agreement with the identified HCC in the observed

351   range of pressure heads. All three models result in a more realistic estimate of the HCC compared to the simple linear

352   scaling approach. While the model of Novák slightly underestimates the identified HCC for all the four RF contents,

353   the results are contrary for the GEM model where the reduction in the hydraulic conductivity is overestimated. The

354   Maxwell model shows the same results as GEM model except for the stony soil with $f = 37.3\,\%$ where it

355   underestimates the HCC.

356   In order to compare the performance of the three models, the average deviation (d_{avg}) between the calculated and

357   identified HCC (logarithmic scale) was calculated to quantify the error of each model in the pF range 0 to 3 (Table

358   3). The signs of numbers in Table 3 represent the tendency of the model in over- or underestimating the identified

359   hydraulic conductivities. The negative sign means the model underestimates the reduction of hydraulic conductivity.

360   *Table 3: Performance of the Novák, Maxwell and GEM models quantified by the average deviation hydraulic conductivities*
361   *(d_{avg}) in logarithmic scale for different values of f.*

model	Volumetric fraction of RF, f (%)			
	11.0	19.8	28.5	37.3
Novák	-0.0068	-0.0028	-0.0179	-0.0231
Maxwell	0.0056	0.0162	0.0039	-0.0038
GEM	0.0077	0.0234	0.0197	0.0248

362

363   Table 3 confirms the qualitative tendency of underestimation of the conductivity reduction by the Novák model and

364   the overestimation by the GEM and Maxwell models, but also shows that the difference between the three models is

365   not large and probably not of relevance in practice (the GEM model at the high value of f, which has the highest

366   deviation, corresponds to a relative mismatch of hydraulic conductivities about 6 %). However, despite the potential

367   of the three models in predicting the HCC of stony soils, we think they require further evaluations using field measured

368   data of hydraulic conductivity in different experimental conditions.

369   **4. Conclusions**

370   In this study, we created virtual stony soils with different volumetric fractions of RF in 3D and identified their effective

371   SHP from saturation up to $pF = 3$ by inverse modeling of virtual EVA and MSUG experiments in 1D. We used the

372   identified SHP to investigate the performance of the available scaling models in stony soils, namely the Bouwer and

373   Rice (1984) model of scaling the WRC, and Ravina and Magier (1984), Maxwell (Peck and Watson, 1979), Novák

374   (Novák et al., 2011), and GEM (Naseri et al., 2020) models for scaling HCC of stony soils.

375   Our results show that the boundary fluxes and the internal system states in the virtual 3D EVA experiments,

376   represented by the observed time series of pressure heads at multiple depths, could be matched well by 1D simulations,

377   and the effective WRC and HCC of the considered stony soils were determined accurately. Comparison with the

378   scaling models showed that by assuming a homogeneous background soil and impermeable RF, the effective WRC

379   can be calculated from the WRC of the background soil using a simple correction factor equal to the volume fraction

380   of background soil, $(1 - f)$. That is a result with practical implications in obtaining WRC of stony soils. In addition,

381   the scaling results for HCC were promising. Our results confirmed that the reduction in K_r was stronger than calculated

382   by a simple proportionality to $(1 - f)$. The three models of Novák, Maxwell, and GEM consider that and performed

383   adequately in predicting the effective HCC of stony soils. The Maxwell model matched the numerical results best.

384   Care must be taken before generalizing these results to arbitrary conditions, e.g., highly dynamic boundary conditions

385   with sequences of precipitation and higher and lower evaporation rates, which might yield different results due to the

386   occurrence of non-equilibrium water dynamics and hysteresis. For real stony soils, changes in the pore size distribution

387   of the background soil may result from the presence of RF (Sekucia et al., 2020) with corresponding consequences

388   for effective SHP. This influence was reported to be more common in compactable soils with a shrinkage-swelling

389   potential (Fiès et al., 2002). In highly stony soils, where RF are not embedded completely in the background soil, the

390   existence of effective SHP is still an open question. Finally, the impact of arrangement and size of RF on evaporation

391   dynamics and effective SHP needs to be understood. Tackling these problems requires a combination of experimental

392   and modelling approaches.

393   **References**

394 Abbasi, F., Jacques, D., Šimůnek, J., Feyen, J., and Van Genuchten, M.T.: Inverse estimation of soil hydraulic and
395 solute transport parameters from transient field experiments: Heterogeneous soil, Transactions of the ASAE, 46(4),
396 1097, doi: 10.13031/2013.13961, 2003.

397 Arias, N., Virto, I., Enrique, A., Bescansa, P., Walton, R., and Wendroth, O.: Effect of Stoniness on the Hydraulic
398 Properties of a Soil from an Evaporation Experiment Using the Wind and Inverse Estimation Methods, Water, 11(3),
399 440, doi: 10.3390/w11030440, 2019.

400 Ballabio, C., Panagos, P., and Monatanarella, L.: Mapping topsoil physical properties at European scale using the
401 LUCAS database, Geoderma, 261, 110-123, doi: 10.1016/j.geoderma.2015.07.006, 2016.

402 Beckers, E., Pichault, M., Pansak, W., Degré, A., and Garré, S.: Characterization of stony soils´ hydraulic conductivity
403 using laboratory and numerical experiments, Soil, 2, 421– 431, doi: 10.5194/soil-2-421-2016, 2016.

404 Bouwer, H., and Rice, R.C.: Hydraulic properties of stony vadose zones, Ground Water, 22, 696–705, doi:
405 10.1111/j.1745-6584.1984.tb01438.x, 1984.

406 Brakensiek, D.L., Rawls, W.J., and Stephenson, G.R.: Determining the saturated conductivity of a soil containing rock
407 fragments, Soil Sci. Soc. Am. J., 50, 834-835, doi: 10.2136/sssaj1986.03615995005000030053x, 1986.

408 Celia, M.A., Bouloutas, E.T. and Zarba, R.L.: A general mass-conservative numerical solution for the unsaturated
409 flow equation, Water Resour. Res., 26(7), 1483-1496, doi: 10.1029/WR026i007p01483, 1990.

410 Coppola, A., Dragonetti, G., Comegna, A., Lamaddalena, N., Caushi, B., Haikal, M.A., and Basile, A.: Measuring
411 and modeling water content in stony soils, Soil Till. Res., 128, 9-22, doi: 10.1016/j.still.2012.10.006, 2013.

412 Corwin, D.L., and Lesch, S.M.: Apparent soil electrical conductivity measurements in agriculture, Comput. Electron.
413 Agr., 46 (1-3), 11-43, doi: 10.1016/j.compag.2004.10.005, 2005.

414 Cousin, I., Nicoullaud, B., and Coutadeur, C.: Influence of rock fragments on the water retention and water percolation
415 in a calcareous soil, Catena, 53: 97–114, doi: 10.1016/S0341-8162(03)00037-7, 2003.

416 Dann, R., Close, M., Flintoft, M., Hector, R., Barlow, H., Thomas, S., and Francis, G.: Characterization and estimation
417 of hydraulic properties in an alluvial gravel vadose zone, Vadose Zone J., 8(3), 651-663, doi: 10.2136/vzj2008.0174,
418 2009.

419 Durner, W., and Flühler, H.: Chapter 74: Soil hydraulic properties, in M. G. Anderson, and J. J. McDonnell (Eds.), in:
420 Encyclopedia of hydrological sciences, chapter 74, 1103–1120. John Wiley & Sons.,
421 doi:10.1002/0470848944.hsa077c, 2006.

422 Durner, W., and Iden, S.C.: Extended multistep outflow method for the accurate determination of soil hydraulic
423 properties near water saturation, Water Resour. Res., 47(8), doi: 10.1029/2011WR010632, 2011.

424 Durner, W., Jansen, U., and Iden, S.C.: Effective hydraulic properties of layered soils at the lysimeter scale determined
425 by inverse modelling, Euro. J. Soil Sci., 59(1), 114-124, doi: 10.1111/j.1365-2389.2007.00972.x, 2008.

426 Farthing, M.W., and Ogden, F.L.: Numerical solution of Richards' equation: A review of advances and challenges,
427 Soil Sci. Soc. Am. J., 81(6), 1257-1269, doi: 10.2136/sssaj2017.02.0058, 2017.

428 Fiès, J.C., Louvigny, N.D.E., and Chanzy, A.: The role of stones in soil water retention, Euro. J. Soil Sci., 53(1), 95-
429 104, doi: 10.1046/j.1365-2389.2002.00431.x, 2002.

430 Germer, K., and Braun J.: Determination of anisotropic saturated hydraulic conductivity of a macroporous slope soil,
431 Soil Sci. Soc. Am. J., 79, 1528-1536, doi: 10.2136/sssaj2015.02.0071, 2015.

432 Grath, S.M., Ratej, J., Jovičić, V., and Curk, B.: Hydraulic characteristics of alluvial gravels for different particle sizes
433 and pressure heads, Vadose Zone J., 14 (3), doi: 10.2136/vzj2014.08.0112, 2015.

434 Haghverdi, A., Öztürk, H.S., and Durner, W.: Measurement and estimation of the soil water retention curve using the
435 evaporation method and the pseudo continuous pedotransfer function, J. hydrol., 563, 251-259, doi:
436 10.1016/j.jhydrol.2018.06.007, 2018.

437 Hlaváčiková, H., and Novák V.: A relatively simple scaling method for describing the unsaturated hydraulic functions
438 of stony soils, J. Plant Nutr. Soil Sci., 177, 560–565, doi: 10.1002/jpln.201300524, 2014.

439 Hlaváčiková, H., Novák V., and Šimůnek J.: The effects of rock fragment shapes and positions on modeled hydraulic
440 conductivities of stony soils, Geoderma, 281, 39–48, doi: 10.1016/j.geoderma.2016.06.034, 2016.

22

441 Hlaváčiková, H., Novák, V., Kostka, Z., Danko, M., and Hlavčo, J.: The influence of stony soil properties on water
442 dynamics modeled by the HYDRUS model, J. Hydrol. Hydromech., 66(2), 181-188, doi: 10.1515/johh-2017-0052,
443 2018.

444 Hopmans J.W., Šimůnek J., Romano N., and Durner W.: Inverse Modeling of Transient Water Flow, in: Methods of
445 Soil Analysis, Part 1, Physical Methods, Chapter 3.6.2, Eds. J. H. Dane and G. C. Topp, Third edition, SSSA, Madison,
446 WI, 963–1008, 2002.

447 Kutilek, M.: Soil hydraulic properties as related to soil structure, Soil and Tillage Research, 79(2), 175-184, doi:
448 10.1016/j.still.2004.07.006, 2004.

449 Lai, J., and Ren, L.: Estimation of effective hydraulic parameters in heterogeneous soils at field scale, Geoderma, 264,
450 28-41, doi: 10.1016/j.geoderma.2015.09.013, 2016.

451 Lehmann, P., Bickel, S., Wei, Z., and Or, D.: Physical constraints for improved soil hydraulic parameter estimation
452 by pedotransfer functions, Water Resour. Res., 56(4), e2019WR025963, doi: 10.1029/2019WR025963, 2020.

453 Mualem, Y.: A new model for predicting the hydraulic conductivity of unsaturated porous media, Water Resour. Res.,
454 12, 513–521, doi: 10.1029/WR012i003p00513, 1976.

455 Naseri, M., Iden, S. C., Richter, N., and Durner, W.: Influence of stone content on soil hydraulic properties:
456 experimental investigation and test of existing model concepts, Vadose Zone J., 18(1), 1-10., doi:
457 10.2136/vzj2018.08.0163, 2019.

458 Naseri, M., Peters, A., Durner, W., and Iden, S.C.: Effective hydraulic conductivity of stony soils: General effective
459 medium theory, Adv. Water Resour., 146, 103765, doi: 10.1016/j.advwatres.2020.103765, 2020.

460 Nasta, P., Huynh, S., and Hopmans, J.W.: Simplified multistep outflow method to estimate unsaturated hydraulic
461 functions for coarse-textured soils, Soil Sci. Soc. Am. J., 75(2), 418-425, doi: 10.2136/sssaj2010.0113, 2011.

462 Novák, V., and Hlaváčiková, H.: Applied Soil Hydrology, Springer International Publishing, doi: 10.1007/978-3-030-
463 01806, 2019.

464 Novák, V., Kňava, K., and Šimůnek, J.: Determining the influence of stones on hydraulic conductivity of saturated
465 soils using numerical method, Geoderma, 161, 177–181. doi: 10.1016/j.geoderma.2010.12.016, 2011.

466 Peters, A., and Durner, W.: Simplified evaporation method for determining soil hydraulic properties, J. Hydrol., 356
467 (1-2), 147-162, doi: 10.1016/j.jhydrol.2008.04.016, 2008.

468 Peters, A., Iden, S.C., and Durner, W.: Revisiting the simplified evaporation method: Identification of hydraulic
469 functions considering vapor, film and corner flow, J. Hydrol., 527, 531-542, doi: 10.1016/j.jhydrol.2015.05.020, 2015.

470 Peters, R. R., and Klavetter, E. A.: A continuum model for water movement in an unsaturated fractured rock mass,
471 Water Resour. Res., 24, 416–430, doi: 10.1029/WR024i003p00416, 1988.

472 Ponder, F., and Alley, D.E.: Soil sampler for rocky soils. US Department of Agriculture, Forest Service, North Central
473 Forest Experiment Station, 1997.

474 Radcliffe, D.E., and Šimůnek, J.: Soil physics with HYDRUS: Modeling and applications. CRC press, 2018.

475 Ravina, I., and Magier, J.: Hydraulic conductivity and water retention of clay soils containing coarse fragments, Soil
476 Sci. Soc. Am. J., 48(4), 736-740., doi: 10.2136/sssaj1984.03615995004800040008x, 1984.

477 Russo, D.: Determining soil hydraulic properties by parameter estimation: On the selection of a model for the hydraulic
478 properties, Water Resour. Res., 24(3), 453-459, doi: 10.1029/WR024i003p00453, 1988.

479 Sarkar, S., Germer, K., Maity, R., and Durner, W.: Measuring near-saturated hydraulic conductivity of soils by quasi
480 unit-gradient percolation—1. Theory and numerical analysis, J. Plant Nutr. Soil Sc., 182(4), 524-534, doi:
481 10.1002/jpln.201800382, 2019.

482 Schelle, H., Iden, S.C., Peters, A., and Durner, W.: Analysis of the agreement of soil hydraulic properties obtained
483 from multistep-outflow and evaporation methods, Vadose Zone J., 9(4), 1080-1091, doi: 10.2136/vzj2010.0050, 2010.

484 Schelle, H., Durner, W., Schlüter, H., Vogel, H.-J., and Vanderborght, J.: Virtual Soils: Moisture measurements and
485 their interpretation by inverse modeling, Vadose Zone J., 12:3, doi: 10.2136/vzj2012.0168, 2013.

486 Schindler, U., Durner, W., von Unold, G., and Müller, L.: Evaporation method for measuring unsaturated hydraulic
487 properties of soils: Extending the measurement range, Soil Sci. Soc. Am. J., 74(4), 1071-1083, doi:
488 10.2136/sssaj2008.0358, 2010.

489 Schofield, R.K.: The pF of water in soil, in: Trans. of the Third International Congress on Soil Science, 2, Plenary
490 Session Papers, 30 July-7 August, 1935 Oxford, UK, pp. 37-48, 1935.

491 Sekucia, F., Dlapa, P., Kollár, J., Cerdá, A., Hrabovský, A., and Svobodová, L.: Land-use impact on porosity and
492 water retention of soils rich in rock fragments, CATENA, 195, 104807, doi: 10.1016/j.catena.2020.104807, 2020.

493 Šimůnek, J., Van Genuchten, M.T., and Šejna, M.: The HYDRUS software package for simulating two-and three-
494 dimensional movement of water, heat, and multiple solutes in variably-saturated media, Technical manual, version,
495 1, 241, 2006.

496 Šimůnek, J., van Genuchten, M.T., and Šejna, M.: Development and applications of the HYDRUS and STANMOD
497 software packages and related codes, Vadose Zone J., 7(2), 587-600, doi: 10.2136/vzj2007.0077, 2008.

498 Šimůnek, J., Van Genuchten, M.T., and Šejna, M.: Recent developments and applications of the HYDRUS computer
499 software packages, Vadose Zone J., 15(7), doi: 10.2136/vzj2016.04.0033, 2016.

500 Singh, A., Haghverdi, A., Öztürk, H.S., and Durner, W.: Developing Pseudo Continuous Pedotransfer Functions for
501 International Soils Measured with the Evaporation Method and the HYPROP System: I. The Soil Water Retention
502 Curve, Water, 12(12), 3425, doi: 10.3390/w12123425, 2020.

503 Singh, A., Haghverdi, A., Öztürk, H.S., and Durner, W.: Developing Pseudo Continuous Pedotransfer Functions for
504 International Soils Measured with the Evaporation Method and the HYPROP System: II. The Soil Hydraulic
505 Conductivity Curve, Water, 13(6), 878, doi: 10.3390/w13060878, 2021.

506 Stevenson, M., Kumpan, M., Feichtinger, F., Scheidl, A., Eder, A., Durner W., and Strauss, P.: Innovative method for
507 installing soil moisture probes in a large-scale undisturbed gravel lysimeter, Vadose Zone J., 1–7, doi:
508 10.1002/vzj2.20106, 2021.

509 Tetegan, M., de Forges, A.R., Verbeque, B., Nicoullaud, B., Desbourdes, C., Bouthier, A., Arrouays, D., and Cousin,
510 I.: The effect of soil stoniness on the estimation of water retention properties of soils: A case study from central
511 France, Catena, 129, 95-102, doi: 10.1016/j.catena.2015.03.008, 2015.

512 Van Genuchten, M.T.: A closed-form equation for predicting the hydraulic conductivity of unsaturated soils, Soil Sci.
513 Soc. Am. J., 44, 892-898, doi: 10.2136/sssaj1980.03615995004400050002x, 1980.

514 Verbist, K.M.J., Cornelis, W.M., Torfs, S., and Gabriels, D.: Comparing methods to determine hydraulic
515 conductivities on stony soils, Soil Sci. Soc. Am. J., 77(1), 25-42, doi: 10.2136/sssaj2012.0025, 2013.

516 Wang, W., Sun, L., Wang, Y., Wang, Y., Yu, P., Xiong, W., Shafeeque, M., and Luo, Y.: A convex distribution of
517 vegetation along a stony soil slope due to subsurface flow in the semiarid Loess Plateau, northwest China, J. Hydrol.,
518 586, 124861, doi: 10.1016/j.jhydrol.2020.124861, 2020.

519 Zhang, Y., Zhang, M., Niu, J., Li, H., Xiao, R., Zheng, H., and Bech, J.: Rock fragments and soil hydrological
520 processes: significance and progress, Catena, 147, 153-166, doi: 10.1016/j.catena.2016.07.012, 2016.

521 Zimmerman, R. W., and Bodvarsson, G.S.: The effect of rock fragments on the hydraulic properties of soils. Lawrence
522 Berkeley Lab., CA, USA, USDOE, Washington, D.C., USA, doi: 10.2172/102527, 1995.